Inhibition of both mutant and wild-type RAS-GTP in KRAS G12C colorectal cancer through cotreatment with G12C and EGFR inhibitors

Thomas McFall[1], Michael Trogdon[1], Laura Sisk-Hackworth[1], Edward C. Stites[1]*

[1] Integrative Biology Laboratory, Salk Institute for Biological Studies, La Jolla, CA 92037, USA.

[*] Corresponding author. Email: estites@salk.edu

Abstract

Multiple KRAS G12C inhibitors are in development, and the identification of effective combination treatment regimens should maximize the benefit these agents have on cancer patients. Here, we find that KRAS G12C heterozygous mutated colorectal cancer cells are sensitive to targeting with EGFR therapeutic antibodies. We find that KRAS G12C is partially impaired in binding to tumor suppressor NF1 and also to RAF, and our computational simulations reveal how these deficiencies result in partial sensitivity to EGFR inhibition. For the combination of EGFR and G12C inhibitors we observe synergy and reductions in active forms of both wild-type and mutant RAS. Our simulations reveal the synergy involves both wild-type and mutant RAS. Overall, our work suggests that the addition of an EGFR inhibitor to a KRAS G12C inhibitor regimen should be further evaluated as a strategy for KRAS G12C colorectal cancer patients.

INTRODUCTION

Both of the anti-EGFR humanized antibodies cetuximab and panitumumab have demonstrated survival benefit for colorectal cancer (CRC) patients (*1, 2*). The RAS GTPases are essential intermediate components in the signaling network that transmits signals from EGFR to the RAF/MEK/ERK cascade that drives cellular proliferation (*3*). Nearly 40% of colorectal cancers have a mutant form of KRAS (*4*) that is constitutively active and drives increased signaling through RAF/MEK/ERK, even in the absence of upstream EGFR activation. It has been shown in clinical trials that the subset of colorectal cancer patients who have any KRAS mutation at codon 12 or 13 (the two major KRAS mutation "hot spots") do not benefit from these EGFR agents (*4*).

The constitutively active KRAS G12C mutant, in which the Glycine (G) residue at codon 12 is replaced with a Cysteine (C), is the most common KRAS mutant in lung cancer (*5-8*), and the fourth most common KRAS mutant in colorectal cancer (*7-9*). A major advance in RAS biology has been the development of small molecules that can covalently interact specifically with this Cysteine residue that is unique to the G12C mutant (*10, 11*), thus conferring the long-sought ability to pharmaceutically target mutant, but not wild-type, RAS (*3*). Some of these agents are now in clinical trials, and early reports are promising (*12, 13*). However, there is also the expectation that KRAS G12C inhibitors will need to be used in combination regimens. The identification of effective combination regimens is therefore a pressing need in RAS cancer medicine.

We have recently solved the problem of why KRAS G13D, in which the Glycine residue at codon 13 is replaced with an Aspartic Acid (D), and is the third most common KRAS mutant in colorectal cancer, is an exception to the rule that KRAS mutations confer resistance to the EGFR inhibitor cetuximab (*14*). The original clinical observation that patients with this mutation benefitted from cetuximab was published nearly a decade ago (*15*) and perplexed RAS biologists and clinicians, who struggled to identify a mechanism that could explain why cancers with a KRAS mutant that is constitutively active in an EGFR-independent manner would respond to an EGFR inhibitor. Through mathematical modeling that leveraged available biochemical and biophysical data on KRAS mutants and experimental cancer cell biology, we revealed that EGFR inhibitors like cetuximab can inhibit wild-type RAS-GTP (predominantly HRAS and NRAS) in

some colorectal cancer cells with KRAS mutations, and that the determinative property is whether or not the KRAS mutant interacts with tumor suppressor NF1 (*14*).

Here, we investigate whether EGFR inhibitors may be an effective combination with KRAS G12C inhibitors in colorectal cancer, and whether there may be a contribution from wild-type RAS-GTP inhibition to complement the inhibition of the G12C mutant. Experimentally, we find that KRAS G12C heterozygous mutant CRC cells, but not homozygous mutant cells, are partially sensitive to cetuximab. We detected impaired binding of KRAS G12C to both NF1 and the Ras Binding Domain (RBD) from CRAF (*RAF1*). Our mathematical modeling suggests these deficiencies are consistent with partial sensitivity to cetuximab. Experimentally, we detected synergy in the combination of cetuximab and KRAS G12C inhibitor AMG-510. Our mathematical model also suggests that synergy exists for combinations of EGFR and G12C inhibitors, and that it comes from the effects of the combination on inhibiting wild-type RAS in addition to KRAS G12C. Experimentally, we observe combination treatment decreases GTP-bound RAS for both wild-type RAS (HRAS and NRAS) and KRAS. Overall, this work suggests patients with KRAS G12C mutant colorectal cancer should be evaluated for possible benefit from EGFR inhibitors, including as part of a regimen with covalent G12C inhibitors should they gain regulatory approval.

RESULTS

Heterozygous mutant KRAS G12C CRC cells are sensitive to EGFR inhibition

To investigate whether the EGFR inhibitor cetuximab might have activity on KRAS G12C CRC we first utilized a panel of isogenic CRC cells derived from the SW48 colon cancer cell line. Through homologous recombination, multiple derivative cell lines are available that have one KRAS allele replaced with a KRAS mutant allele (*14-16*). We performed cetuximab dose responses on SW48 KRAS WT cells, as well KRAS G12C, KRAS G12V, and KRAS G12D derivative isogenics. Our MTT drug dose response experiments found KRAS G12C cells were sensitive to cetuximab, like KRAS WT and unlike KRAS G12V and KRAS G12D cells (**Figure 1A**). We confirmed this with a cell counting assay (**Figure 1B**).

To investigate whether these findings would generalize to other CRC cell lines, we obtained two KRAS G12C CRC cell lines: SW837 (heterozygous KRAS G12C mutant) and SW1463 (homozygous KRAS G12C mutant) (*12*). We observed SW837 cells to be sensitive to

cetuximab (IC50 of 0.793 μM) but not the SW1463 cells (**Figure 1C**). We also performed our cell counting assay to confirm the proliferation differences suggested by the MTT assays. We found heterozygous mutant SW837 cells displayed reduced proliferation with cetuximab treatment, while homozygous mutant SW1463 cells displayed no change in proliferation upon treatment with cetuximab (**Figure 1D**).

EGFR inhibition results in reduced wild-type HRAS and NRAS activation in G12C CRC

Our previous studies that investigated the response of KRAS G13D CRC cells to EGFR inhibition found that, upon EGFR inhibition, sensitive G13D cells display a reduction in HRAS-GTP and NRAS-GTP (which is all wild-type in these cells), but not in mutant KRAS-GTP. In contrast, we found that KRAS G12D and G12V lines do not display reductions in HRAS-GTP or NRAS-GTP upon treatment with cetuximab (*14*). We hypothesized that the sensitivity of the G12C line also follows from reductions in wild-type RAS-GTP, but not in mutant KRAS-GTP.

To investigate, we treated SW48 G12C, G12V and WT cells with and without cetuximab and then utilized RBD pull-down to isolate active RAS-GTP. We then performed Western blotting on the pull-down lysates with antibodies individually specific for HRAS, NRAS, and KRAS (RBD-WB). Our immunoblots detected reduced wild-type HRAS and wild-type NRAS in the RBD lysates from G12C CRC cells after treatment with cetuximab, but no major change was detected in KRAS levels, consistent with our hypothesis (**Figure 2A and 2B**). Additionally, immunoblots of whole-cell lysate observed reduced phosphorylated ERK, suggesting that reductions in wild-type RAS-GTP result in reduced downstream signaling (**Figure 2A and 2C**).

To thoroughly investigate the changes in GTP-bound RAS in HRAS, NRAS, and KRAS forms, we used isoelectric focusing to separate the HRAS, NRAS, and KRAS on the basis of their isoelectric point differences. We performed isoelectric focusing on RBD-pulldown lysates in cetuximab treated and untreated cells and then immunoblotted with a pan-RAS antibody (RBD-IEF). These experiments confirmed reductions in wild-type HRAS and wild-type NRAS in KRAS G12C SW48 cells (**Figure 2D and 2E**), consistent with our hypothesized mechanism. We also observed reductions in wild-type HRAS, NRAS, and KRAS in KRAS WT SW48 cells and no major change in wild-type HRAS or NRAS in KRAS G12V SW48 cells (**Figure 2D and 2E**), all consistent with our hypothesis.

We validated these findings in our other KRAS G12C cell lines. Our RBD pull-downs detected reduced HRAS-GTP and NRAS-GTP by RBD-WB in G12C heterozygous mutant SW837 cells upon treatment with cetuximab (**Figure 2F and 2G**). The whole-cell lysates treated with cetuximab also displayed reduced ERK phosphorylation (**Figure 2F and 2H**). In contrast, the G12C homozygous mutant SW1463 cells that did not display sensitivity to cetuximab had no major change in HRAS-GTP or NRAS-GTP by RBD-WB (**Figure 2F and 2G**) and no change in ERK phosphorylation (**Figure 2F and 2H**). Similarly, evaluation of RAS GTP in its various forms by RBD-IEF detected reductions in HRAS-GTP and NRAS-GTP for SW837 heterozygous G12C mutant cells but not SW1463 homozygous G12C mutant cells (**Figure 2I and 2J).**

KRAS G12C binds less well to NF1 than KRAS G12V and KRAS WT

Our previous studies established that KRAS G13D CRC cells respond to EGFR inhibition due to a reduced affinity between KRAS and NF1. Strongly interacting, constitutively active RAS mutants cannot be inactivated by NF1, but their non-productive interaction with the NF1 GAP domain effectively results in a competitive inhibition of NF1 and thereby leads to increased wild-type RAS-GTP in an EGFR-independent manner. Mutants like KRAS G13D that weakly interact with NF1 do not strongly drive wild-type RAS-GTP production through NF1 competitive inhibition and therefore can remain dependent upon EGFR for WT RAS-GTP generation (*14*). We hypothesized that the sensitivity of G12C also follow from reductions in binding to NF1 for the KRAS G12C mutant.

We utilized Bioluminescent Resonance Energy Transfer (BRET) to characterize interactions between different KRAS mutants with full-length NF1. We observed KRAS G12C to interact with NF1 much less strongly than KRAS G12V and KRAS WT (**Figure 3A and 3B**). The decrease observed was not as profound as the decrease we previously observed for KRAS G13D binding to NF1 (*14*).

To validate these results, we utilized a co-immunoprecipitation assay that used pooled lysates from NF1 and KRAS mutant transfected cells. We performed our co-immunoprecipitation assay after bathing the KRAS lysates with non-hydrolyzable GTP for 20 minutes before mixing with NF1 lysates and then coimmunoprecipitating. In these conditions, WT Ras binds strongly to NF1, suggesting that the pre-treatment with non-hydrolyzable

treatment was effective at promoting the GTP-bound conformation (**Figure 3C and 3D**). In these conditions, KRAS G12C displayed less binding to NF1 compared to KRAS G12V and KRAS WT, consistent with what was observed in our BRET assays (**Figure 3C and 3D**).

KRAS G12C binds less well to the CRAF

We noted that the proportions of KRAS to NRAS and of KRAS to HRAS in the RBD-pulldown IEF experiment was different from what was observed for other KRAS mutants (i.e. Figure 2D). In our previous work with these SW48 cells we usually find approximately 50% of the RAS on an IEF blot to be KRAS with the remainder split between HRAS and NRAS. In contrast, our IEF on SW48 G12C cells found nearly even levels of KRAS, NRAS, and HRAS (i.e. Figure 2E). We considered two possible explanations: that KRAS G12C binds less well to RBD, or that the KRAS G12C SW48 isogenic clone has different proportions of total KRAS, NRAS, and HRAS than is found in the other SW48 isogenic cells. To evaluate, we performed isoelectric focusing on the total cell lysates from G12C, G12V, and WT, SW48 cells for both cetuximab treated and untreated cells (**Figure 3E**). We reproducibly observed much more similar proportions of KRAS to NRAS and of KRAS to HRAS between these whole cell lysates (**Figure 3F**). This suggests that the levels of KRAS, NRAS, and HRAS are similar between the isogenic cell lines. This is also consistent with pervious proteomic characterization of these cells (*16*).

We also investigated whether the proportion of KRAS to NRAS and of KRAS to HRAS varies between whole cell lysates and RBD lysates in the SW837 and SW1463 G12C CRC cells. IEF blots of whole cell lysates from these cell lines (**Figure 3G**) reproducibly revealed a higher proportion of total RAS in the KRAS form than was observed by RBD-IEF (**Figure 3H**). Of note, the proportion of KRAS to NRAS and of KRAS to HRAS varied between SW48, SW837, and SW1463 cells, although the proportions were similar within the SW48 isogenics (**Figure 3F and 3H**).

The comparison between our whole cell lysate IEF and our RBD-IEF suggests that KRAS G12C-GTP binds to the RBD less well than the other KRAS mutants. To test this hypothesis, we utilized BRET. Our BRET experiment found KRAS G12C bound less well to CRAF-RBD than KRAS WT and KRAS G12V (**Figure 3I and 3J**). To confirm, we compared RBD pulldowns of KRAS between isogenic KRAS G12C, KRAS G12V, and KRAS WT SW48

cells. We detected reduced binding of KRAS G12C to RBD relative to KRAS G12V (**Figure 3K and 3L**). We also detected no KRAS WT binding, consistent with low levels of RAS-GTP in unstimulated KRAS WT cells. Incubation of cell lysates from the different SW48 cells with non-hydrolyzable GTP prior to the RBD precipitations resulted in an increased binding of WT RAS to the RBD, indicating successful loading of the non-hydrolyzable GTP analogue. In these conditions, our immunoblots continued to find decreased binding of G12C to RBD relative to G12V and WT RAS (**Figure 3K and 3L**), suggesting that differences in the proportion of GTP-bound forms of the KRAS mutant did not explain the differences observed. Altogether, these studies suggest that GTP-bound G12C binds less well to the RBD from CRAF.

Modeling supports Ras signaling complex observations

Our previous finding that EGFR inhibitors like cetuximab can reduce WT HRAS-GTP and NRAS-GTP in KRAS G13D CRC cells was first uncovered by our mathematical modeling (*17*). Our mathematical model of oncogenic RAS signaling was developed to be capable of modeling specific RAS mutant alleles on the basis of their kinetic, equilibrium, and enzymatic biochemical parameters for the reactions that regulate RAS-GTP cycling (*18-20*).

Our work here on KRAS G12C similarly observes sensitivity to EGFR inhibitors. Whether this sensitivity is explained by the partial reduction in impaired NF1 binding relative to KRAS G13D, and/or by reduced binding to RAS effectors, and whether zygosity modulates, are features that we can investigate with our mathematical model.

Previously, we performed a computational analysis of KRAS G12C and its response to G12C covalent inhibitors (*21*). That study utilized published biochemical rate constants for KRAS G12C (*22*); however, the data available at that time did not characterize the interaction between KRAS G12C and NF1, and we thus originally modeled KRAS G12C to bind to NF1 equivalently to KRAS WT and KRAS G12V. Now that we have new information on this interaction (e.g. Figure 3A) updating our parameters to reflect reduced binding to NF1 is warranted.

Simulations with our original KRAS G12C parameters would suggest that KRAS G12C responds to cetuximab like KRAS G12V and would therefore be insensitive (**Figure 4A**). However, once our KRAS G12C parameters were updated to reflect the decreased binding to

NF1, as observed with our BRET assay, the model suggests cells with the G12C mutant would be more sensitive to EGFR (**Figure 4A**).

Both the original and updated G12C parameters would suggest that there is no major change to the level of GTP-bound mutant KRAS G12C upon EGFR inhibition (**Figure 4B**). The model also suggests that KRAS G12C CRC cells should show a reduction in WT RAS-GTP comparable to what is observed for KRAS WT and KRAS G13D conditions when the updated, NF1-binding impaired, parameters are utilized (**Figure 4B**). We utilize the impaired NF1-binding parameterized G12C mutant going forward, as this best reflects our experimental characterization of the G12C-NF1 interaction and is most consistent with our signaling and drug response observations.

We then considered what the model would anticipate for heterozygous and homozygous G12C mutations. To model heterozygous conditions, we modeled 25% of total cellular RAS to be the G12C mutant, and to model the homozygous conditions, we modeled 50% of total cellular RAS to be the G12C mutant. This reflects approximately 50% of total cellular RAS being KRAS, which is the value we have used previously in our simulations (*14*). The model suggests that the heterozygous mutant condition would respond to EGFR inhibition like the G13D (sensitive) cancer cells and that the homozygous mutant condition would respond to EGFR inhibition like the G12V (resistant) cancer cells (**Figure 4C**). This suggests that the resistance of SW1463 homozygous G12C mutant cells and the sensitivity of SW837 heterozygous G12C mutant cells may be simply explained by the dosage of the G12C mutant within each cell.

Our experiments also detected impaired binding to RAF (e.g. Figure 3I) as well as the impaired binding to NF1. Of note, the previous biophysical characterization of G12C that we previously utilized to parameterize our computational G12C mutant did detect somewhat impaired binding to RBD (*22*) and that value is included in our simulations in Figure 4A and 4B. We set out to evaluate whether reduced binding to RAS effectors would be expected to increase or decrease sensitivity to EGFR inhibition. To do this, we computationally evaluated the consequences of an order of magnitude increase and an order of magnitude decrease in the affinity of KRAS G12C to RAS effectors (**Figure 4D**). We noted that decreased binding to RAS effectors like the RAF kinases should make cells with the G12C mutant less sensitive to EGFR inhibition; that is, reduced binding to RAF and other effectors is predicted to decrease sensitivity to EGFR inhibition. However, we note that the magnitude of this effect was less than observed

for NF1 (Figure 4A vs. Figure 4D) and we also note that the magnitude of change suggested by BRET experiments was less for RAF than for NF1 (Figure 3I vs Figure 3A). Thus, modeling suggests that the reduced binding to RAF may provide a minor modulation of the overall sensitivity to EGFR inhibition that slightly counteracts the effects of reduced NF1 binding.

KRAS G12C covalent inhibition by AMG-510 results in reduced wild-type RAS-GTP, reduced binding to NF1, and reduced binding to CRAF RBD

KRAS G12C covalent inhibitors have recently been developed that appear capable of specifically targeting and inhibiting KRAS G12C (*10-13, 23*). Early reports from clinical trials are promising (*12, 13*). We tested the ability of KRAS G12C inhibitor AMG-510 (*12*) to specifically target KRAS G12C in the CRC cells we have been studying. We performed AMG-510 drug dose responses on these cell lines and observed similar sensitivity to AMG-510 for G12C SW48, SW837, and SW1463 cell lines (**Figure 5A**). In contrast, G12V and WT SW48 cells were insensitive to AMG-510.

Previously described KRAS G12C inhibitors are believed to lock the KRAS G12C in the GDP-bound, inactive state and render it unable to interact with proteins that specifically bind to the GTP-bound conformation of RAS (*23, 24*). We therefore investigated whether the KRAS-G12C protein displayed reduced binding to NF1 and to CRAF RBD after treatment with AMG-510. We tested for these interactions with our BRET assay. We observed KRAS-G12C treated with AMG-510 bound much less strongly to NF1 than KRAS-G12C not treated with AMG-510 (**Figure 5B**). Similarly, we observed KRAS-G12C treated with AMG-510 bound much less strongly to CRAF when compared to vehicle (**Figure 5C**). To confirm, we performed an assay where we evaluate co-immunoprecipitation in mixed cell lysates. We observe that KRAS G12C can be co-immunoprecipitated by NF1, but that treatment with AMG-510 results in KRAS G12C no longer co-immunoprecipitating with NF1 (**Figure 5D and 5E**). Overall, these studies validate that AMG-510 binding to KRAS G12C prevents it from interacting with proteins that normally act with GTP-bound KRAS.

Experiments observe synergy in the combined treatment of KRAS G12C inhibitors with EGFR inhibitors

Previously, it has been empirically shown that co-targeting EGFR along with a G12C inhibitor can result in increased inhibition of the KRAS G12C mutant in lung cancer and pancreatic cancer cell lines (*12, 13, 23-26*). We desired to test this combination in our colorectal cancer cells. We performed drug dose responses that evaluated varying doses of AMG-510 with varying doses of cetuximab. Results for the subset of conditions that had cetuximab alone and that had AMG-510 alone (**Figure 6A**) were consistent with the experiments that evaluated cetuximab alone (Figure 1A,C) and those that evaluated AMG-510 alone (Figure 5A), providing internal controls for our assay.

Our combination treatment experiments detected low levels of proliferation for the combination of EGFR inhibitors with G12C inhibitors for all three of the KRAS G12C mutant cell lines (**Figure 6A**). We calculated the excess over bliss score as a measure of synergy (*27*). We found that there was synergy detected in all three KRAS G12C cell lines, and that the synergy was strongest for the homozygous G12C mutant SW1463 cells (**Figure 6A and 6B**).

Simulations suggest combined treatment of KRAS G12C inhibitors with EGFR inhibitors is synergistic

As KRAS mutations generally confer resistance to EGFR inhibitors, that co-targeting of KRAS G12C cancer cells with both a G12C inhibitor and an EGFR inhibitor would be better than targeting with a G12C inhibitor alone was considered surprising (*28, 29*). The benefit has been attributed to the specificity of G12C inhibitors for the GDP-bound form of RAS and to EGFR inhibition resulting in less GTP-bound RAS mutant (*23, 24*). To our knowledge, a role for WT RAS-GTP has not also been evaluated. As our work here shows a role for WT RAS-GTP depletion by the EGFR inhibitor cetuximab, we wished to evaluate whether some of the benefit from co-treatment with a G12C inhibitor and an EGFR inhibitor follows from targeting WT RAS-GTP.

We applied our computational model to the problem to determine which behavior(s) would be logically consistent with the available biochemical and biophysical data. To simulate the effects of covalent KRAS G12C inhibitors, we utilize a form of our computational model that includes RAS production and degradation (*21*) as these processes are essential for understanding the effects of covalent inhibition. We utilized the updated parameters for KRAS G12C

demonstrated in Figure 4, where we now assume an order of magnitude reduction in binding to NF1 to approximate the observed impairment in binding to NF1.

We simulated combinations of EGFR inhibition (which would result in less SOS mediated GTP-loading of RAS) with different doses of a covalent G12C inhibitor (*23*). We simulated these combinations for both modeled heterozygous mutant conditions and modeled homozygous mutant conditions and considered levels of total RAS-GTP as the model output. Our simulations suggest that there will be considerable amounts of synergy from the combination of an EGFR inhibitor with a G12C covalent inhibitor (**Figure 7A**). The model finds synergy of comparable magnitude in both conditions. Of note, the model suggests that there will be a wider range of synergistic combinations for the homozygous mutant conditions than for the heterozygous mutant conditions.

We wished to determine whether the predicted synergy was from mutant RAS inhibition and/or wild-type RAS inhibition. To do this, we evaluated the predicted levels of mutant RAS-GTP and WT RAS-GTP for the different levels of combined EGFR and G12C inhibition. The model suggests that there will be considerable synergy for both mutant RAS-GTP and WT RAS-GTP. For mutant RAS-GTP, the predicted dose response for KRAS G12C inhibition showed increasing levels of synergy for increasing levels of coincident EGFR inhibition (**Figure 7B**). This is consistent with previous empirical results (*12, 13, 23, 24*) and with our original KRAS G12C modeling (*21*). Additionally, the model suggests that there will also be considerable levels of synergy for WT RAS-GTP (**Figure 7C**). The predicted dose response for EGFR inhibition showed increasing levels of synergy for increasing levels of coincident G12C inhibition. Overall, the model suggests that synergy in the combination of G12C inhibitors and EGFR inhibitors has contributions targeting both from mutant and WT RAS-GTP.

Both wild-type and mutant RAS are targeted by the combination of G12C inhibitors with EGFR inhibitors

We set out to experimentally evaluate how HRAS-, NRAS-, and KRAS-GTP levels change upon treatment with each inhibitor alone and in combination. We focused on the SW837 and SW1463 cells. Cells were treated with either 1μg/ml Cetuximab, 250 nM AMG-510, or both in combination. These doses were based upon synergy studies (Figure 6A and 6B) where at these concentrations alone there was minimal effect on proliferation, but together they had a strong

synergy score. Our RBD-WB experiments revealed no major changes in HRAS-, NRAS-, and KRAS-GTP in homozygous mutant SW1463 cells treated with cetuximab and statistically significant partial reductions in HRAS-, NRAS-, and KRAS-GTP in SW837 cells treated with cetuximab. AMG-510 monotherapy resulted in a partial reduction of HRAS-, NRAS-, and KRAS-GTP in both SW837 and SW1463 cells as well as a partial reduction of phospho-ERK. Furthermore, cetuximab and AMG-510 combination resulted in a robust decrease in HRAS-GTP, NRAS-GTP, and KRAS-GTP (**Figure 8A and 8B**), as well as robust reduction in phospho-ERK signal in both cell lines (**Figure 8A and 8C**). Overall, we found that the combination of the EGFR inhibitor cetuximab with the KRAS G12C inhibitor AMG-510 was able to effectively reduce both wild-type and mutant RAS in the GTP bound form, resulting in decreased ERK phosphorylation.

Kinetic Experiment Reveals the Interplay Between Mutant and Wild-type Ras

We experimentally tested the kinetics of AMG-510 on HRAS-, NRAS-, and KRAS-GTP levels with our RBD-IEF experiment on SW48 G12C cells. We found that KRAS-GTP levels were clearly decreased by 24 and 48 hours, and appeared to display a modest decrease at 12 hours (**Figure 8D**). Additionally, there appears to be a very modest decrease in NRAS-GTP levels by 24 and 48 hours. We would hypothesize that this was the proportion of NRAS-GTP that was promoted by G12C KRAS competitively inhibiting NF1.

We also performed this experiment after 24 hours with cetuximab pre-treatment. At the zero time point of AMG-510, there was already a partial reduction of NRAS-GTP and HRAS-GTP relative to the AMG-510 zero timepoint without cetuximab pre-treatment (**Figure 8D**). As KRAS-GTP levels decreased through the 24 and 48 hour timepoints, the levels of NRAS-GTP and HRAS-GTP further decreased considerably. This demonstrates the mechanism of synergy; as EGFR and mutant are both targeted, all of the mechanisms that promote active, wild-type RAS-GTP in these cells are effectively removed.

DISCUSSION

We here show that KRAS G12C CRC is sensitive to EGFR inhibition and that the combination of EGFR inhibition with KRAS G12C inhibition is synergistic. There is some support for both of these findings in the literature. Studies in lung cancer patient derived

xenografts have suggested KRAS G12C lung cancer may retain benefit from the EGFR and HER2 inhibitor afatinib (*30*). This suggests that sensitivity of KRAS G12C to EGFR inhibition may extend to other cancers, although further work would be required to evaluate whether this is so and whether sensitivity follows from reductions in HRAS-GTP and NRAS-GTP.

Additionally, there is evidence for combined treatment with EGFR inhibitors with KRAS G12C inhibitors. That co-treatment with EGFR inhibitors and KRAS inhibitors would be effective was initially seen as counterintuitive (*28, 29*). However, studies of KRAS G12C inhibitor ARS-853 found that there was improved KRAS targeting from co-treatment with EGFR inhibitors erlotinib and gefitinib in lung cancer cell lines; those studies determined that the blocking of EGFR resulted in impaired GTP-loading of KRAS G12C by RAS GEFs, which in turn facilitated the loading of ARS-853 that necessarily occurs in the GDP bound state (*23, 24*). Two different studies that screened for agents that would synergize with KRAS G12C inhibitors in lung cancer and pancreatic cancer cell lines identified EGFR inhibitors as one possible synergistic target (*25, 26*). The effectiveness of EGFR co-treatment was also attributed to improved KRAS G12C loading due to reduced GTP loading (*26*). A recent publication on AMG510 describes synergy for AMG510 with erlotinib (which targets EGFR) and with aftanib (which targets both EGFR and HER2) as well as with other agents that target downstream of EGFR in lung cancer and pancreatic cancer cell lines. The authors suggested the benefit was attributable to targeting the re-activated EGFR that came from a loss of negative feedback after inhibition of KRAS (*12*). Similarly, a recent publication on the KRAS G12C inhibitor MRTX849 finds the EGFR/HER2 inhibitor afatinib appears useful in combination with MRTX849 in a variety of cell lines (*13*). These other studies substantiate our finding that combination treatment with a G12C inhibitor and an EGFR inhibitor can be an effective combination.

Here, we introduce the idea that co-targeting a KRAS G12C cancer with both a G12C inhibitor and an EGFR inhibitor can effectively reduce both mutant and wild-type RAS signals. To the best of our knowledge, we are the only group to investigate the effects of G12C inhibitor and EGFR inhibitor combinations on WT HRAS and WT NRAS signaling, which we have shown here to be a critical component of the response to combination treatment in colorectal cancer cells. That wild-type RAS signaling is frequently increased in the presence of mutant RAS has extensive experimental evidence (*14, 18, 31-36*), yet it is an aspect of RAS signaling

that is often overlooked when mutant RAS cancers are considered (*37*). We here show that co-targeting wild-type RAS along with mutant RAS may be a valuable strategy for targeting RAS mutant cancers.

Part of our study involved the use of a mathematical model. Mathematical models have played a role in multiple studies of KRAS G12C inhibitors (*21, 23, 38, 39*). Here, we use the model to evaluate the contribution of two biochemical defects of KRAS G12C that were here observed, impaired binding to NF1 and to CRAF, on the observed sensitivity of KRAS G12C cancer cells to EGFR inhibition. The model provides an approach to evaluate which of these two processes is more likely to underlie the empirically observed drug response. We also used the model to evaluate combinations of G12C and EGFR inhibitors, and the model provides an approach to evaluate whether available information on the G12C mutant and these inhibitors are suggestive of there being synergy in their combination. Additionally, the model provides an approach to parse this observed synergy into contributions from the targeting of wild-type RAS and mutant RAS.

Previous uses of mathematical models in G12C inhibitors include evaluating whether observed behaviors are or are not consistent with in vitro data, leading to the realization that there must be a contribution of cellular GEFs to mutant signaling (*23*). Other uses include evaluating how properties of inhibitors and sensitivity to GEF loading are likely to impact loading kinetics (*21, 38, 39*). In all of these models, the ability of mathematical models to relate biochemical processes to cellular observables has been particularly valuable, as inference without a mathematical model can sometimes be challenging for biological networks. For example, the experimental demonstration that GEFs contributed to mutant RAS activation, as shown indirectly with G12C inhibitors that bind to the GDP-bound form of the mutant (*23, 24*), was considered surprising because many in the field had concluded there was no need for GEFs in the GTP loading of oncogenic RAS mutants (*28*). Modeling of the data helped support this finding (*23*). Much earlier computational work on RAS came to the same conclusion that oncogenic RAS maintains some dependency upon GEFs for full activation (*18*). As mathematical and computational models become better accepted in cancer cell biology, perhaps there will be a more rapid adoption of ideas first elucidated via modeling.

We also have revealed that the sensitivity of KRAS G12C cells to the EGFR inhibitor cetuximab has a similar mechanism as what we recently demonstrated for KRAS G13D and its

response to cetuximab (*14*). For the KRAS G13D study, we first used mathematic modeling of available biochemical detect to predict a priori that reductions in wild-type RAS explained the response of KRAS G13D CRC to EGFR inhibition (*17*). In contrast, for this study we first identified KRAS G12C CRC as a genotype that was sensitive to EGFR inhibition empirically, and then we used our mathematical model to evaluate whether the observed deficiencies in the binding of KRAS G12C to NF1 and CRAF, as well as the dependency on the number of KRAS alleles mutated, were consistent with the known mechanisms of RAS signal regulation. We believe that the ability to evaluate whether an observation is or is not logical can be quite powerful. For example, the purely empirical original identification that KRAS G13D CRC was sensitive to cetuximab had not been clinically acted on for nearly a decade, and one stated reason for a lack of action has been that a mechanism to explain why this mutation would behave unlike the others has not been presented (*40*). We both present a mechanism and an assessment of whether or not it is logically consistent with principles of chemical kinetics and RAS GTPase biochemistry, so we hope that the findings presented here are able to make an impact on clinical oncology more quickly than the previous KRAS G13D discoveries.

More generally, the treatment of colorectal cancer with agents that target EGFR, which is upstream from the driver mutation, along with treatments at the level of and/or below the driver mutation, as is suggested here, also has more general precedent. Early studies found that BRAF mutant colorectal cancer did not respond to single agent BRAF inhibitors (*41*). The likely reason for resistance is that targeting BRAF results in loss of negative feedback to the EGFR/RAS/RAF pathway, and that the additional EGFR signals can confound treatment with RAF inhibitors (*42, 43*), possibly due to paradoxical activation of RAF due to the increased wild-type RAS-GTP (*44-46*). Subsequent studies have found BRAF mutant colorectal cancer can benefit from co-treatment with RAF, MEK, and EGFR inhibitors (*47, 48*). It is still unknown whether the benefit from EGFR is solely due to inhibition of wild-type RAS or follows from the other pathways that EGFR can activate (*49*). Overall, the present work further establishes that just because a mutation may cause resistance to a targeted therapy given alone, that same targeted therapy may be able to treat cancers with the “resistance” promoting mutation when it is combined with another targeted therapy.

Materials and Methods

Cell line Models and Culture

SW837, SW1463, SW48 cells and SW48 isogenic counterparts were cultured in RPMI 1640 medium supplemented with fetal bovine serum (FBS) (10%), penicillin (100 U/ml), streptomycin (100 μg/ml), and l-glutamine (2 mM). All cells were grown in indicated medium and incubated at 37°C in 5% CO2 unless indicated otherwise in experimental methods. SW48 cells were obtained from Horizon Discovery. SW837 and SW1463 cells were obtained from the American Type Culture Collection.

Western Blot Analysis

Cell lysates were generated using lysis buffer (Thermo Fisher Scientific, 1862301) containing protease inhibitor cocktail (Cell Signaling Technology) and incubated on ice for 1 hour, with brief vortexing every 5 minutes. The total protein concentration was determined by Pierce Protein assay (Thermo Fisher Scientific). Protein samples were resolved by electrophoresis on 12% SDS–polyacrylamide gels and electrophoretically transferred to polyvinylidene difluoride (PVDF) membranes (Millipore Corporation) for 20 min at 25 V with the Trans-Blot Turbo (Bio-Rad Laboratories). The blots were probed with the appropriate primary antibody and the appropriate fluorophore-conjugated secondary antibody. The protein bands were visualized using the Licor CLx Odyssey imaging station (Licor Biosystems). Comparative changes were measured with Licor Image Studio software from three independent experiments.

Proliferation Assay

Cells (5000 per well) were seeded in 96-well plates in complete media. Treatments were initiated after the cells were attached (24h). At the appropriate time points, cell viability was determined by MTT assay; (5 mg/ml in phosphate-buffered saline) was added to each well followed by incubation at 37°C for 2 hours. The formazan crystal sediments were dissolved in 100 μl of dimethyl sulfoxide, and absorbance was measured at 590 nm using a Tecan Infinite 200 PRO plate reader. Each treatment was performed in eight replicate wells and repeated three different times.

Active RAS Pull-Down Assay

Isolation of active RAS-GTP was performed using the Active Ras Pull-Down and Detection Kit (Thermo Fisher Scientific) following the manufacturer's protocol. RAS abundance was measured by Western blot. Western blot analysis of RBD pull-down lysates was performed with mouse anti-KRAS antibody (WH0003841, Sigma), rabbit anti-NRAS (ab16713, Abcam), rabbit anti-HRAS (18295, Proteintech), mouse anti–pan-RAS antibody (1862335, Thermo Fisher Scientific), and mouse anti-GAPDH (sc-4772, Santa Cruz Biotechnology). Input lysates were analyzed with mouse anti-pERK (675502, Biolegend) and rat anti-ERK (686902, Biolegend).

IEF of Active RAS Isoforms and Total Endogenous RAS

Cells were cultured in T-75 adherent culture flasks. Cells were grown in growth medium alone or growth medium with cetuximab at proper experimental concentration indicated for 48 hours. Medium was removed, and cells were washed with ice-cold tris-buffered saline. Cells were scraped in 1 ml of lysis wash buffer [25 mM tris-HCl (pH 7.2), 150 mM NaCl, 5 mM MgCl2, 1% NP-40, and 5% glycerol]. Cells were lysed on ice and vortexed every 10 s. Cell lysates were subjugated to RBD coimmunoprecipitation as previously described above. RBD coimmunoprecipitation product was resolved by SDS–polyacrylamide gel electrophoresis in a 12% polyacrylamide gel. Bands were excised from the 21-kDa region of the gel. Gel products were liquified at 95°C for 5 min. Protein was extracted and purified using the ReadyPrep 2-D Cleanup Kit (Bio-Rad Laboratories) following the manufacturer's protocol. Protein samples were added to 50% glycerol loading buffer and incubated at room for 20 min. Samples and IEF Ladder were resolved on Criterion Bio-Lyte IEF Gel with a 3 to 10 pH range (Bio-Rad Laboratories). Gels were run at the following power conditions with constant voltage: 100 V for 60 min, 250 V for 60 min, and 500 V for 30 min in a stepwise fashion with a total run time of 150 min. The IEF gel was then soaked in 5% SDS buffer for 24 hours with gentle rocking at 4°C. Protein was electrophoretically transferred to PVDF membranes (Millipore Corporation) for 1 hour at a constant 25 V with Trans-Blot Turbo transfer station (Bio-Rad Laboratories). The PVDF blots were probed with the anti–pan-RAS primary antibody from the Active Ras Pull-Down and Detection Kit (Thermo Fisher Scientific) and the anti-mouse DyLight 800 fluorophore-conjugated secondary antibody (Invitrogen). The protein bands were visualized

using the Licor CLx Odyssey imaging station (Licor Biosystems). Comparative changes were measured with Licor Image Studio software.

NF1 γ-S-GTP Dependent Coimmunoprecipitation

HEK293T cells were individually transfected with the expression plasmid for NF1-Flag, WT KRAS-GFP, G12V KRAS-GFP or G12C KRAS-GFP. Cells were harvested in IP Lysis/Wash Buffer (0.025 M tris-HCl, 0.15 M NaCl, 0.001 M EDTA, 1% NP-40, and 5% glycerol; pH 7.4 and 1× protease inhibitor) 24 hours after transfection. Whole-cell lysates (500 μg) were precleared for 0.5 hours using Control Agarose Resin slurry (Thermo Fisher Scientific). Immunoprecipitation was performed by first incubating 800 μl of HEK293T NF1-Flag precleared lysate with 200 μl of either WT KRAS-GFP, G12V KRAS-GFP or G12C KRAS-GFP precleared cell lysate. Each cell lysate mixture had EDTA (pH 8.0) added to make a final concentration of 10 mM. GTP-γ-S was added to the solution to a final concentration of 100 nM. This solution was incubated at room temperature for 20 min with gentle rocking. The reaction was terminated by adding MgCl2 to the solution at a final concentration of 50 mM. The final steps of the coimmunoprecipitation were performed using the Pierce Immunoprecipitation Kit (Thermo Fisher Scientific) with immobilized anti-NF1 antibody (Santa Cruz Biotechnology, CA). A total of 500 μg of the cell lysate was added and incubated at room temperature under rotary agitation for 2 hours. At the end of the incubation, the complexes were washed five times with lysis buffer. The western blot was probed with mouse monoclonal NF1 antibody (Santa Cruz Biotechnology) and with mouse anti-KRAS antibody (WH0003841, Sigma).

AMG-510 NF1 Coimmunoprecipitation

HEK293T cells were individually transfected or co-transfected with the expression plasmid for NF1-Flag, WT KRAS-GFP, or G12C KRAS-GFP as indicated in Figure 5D. Cells were also simultaneously treated with either vehicle or 500nM of AMG-510 for 24h. Cells were harvested in IP Lysis/Wash Buffer (0.025 M tris-HCl, 0.15 M NaCl, 0.001 M EDTA, 1% NP-40, and 5% glycerol; pH 7.4 and 1× protease inhibitor) 24 hours after transfection and treatment. Whole-cell lysates (500 μg) were precleared for 0.5 hours using Control Agarose Resin slurry (Thermo Fisher Scientific). Immunoprecipitation was performed by first incubating 800 μl of HEK293T NF1-Flag precleared lysate with 200 μl of either WT KRAS-GFP, G12V KRAS-GFP or G12C

KRAS-GFP precleared cell lysate. The final steps of the coimmunoprecipitation were performed using the Pierce Immunoprecipitation Kit (Thermo Fisher Scientific) with immobilized anti-NF1 antibody (Santa Cruz Biotechnology, CA). A total of 500 μg of the cell lysate was added and incubated at room temperature under rotary agitation for 45 m. At the end of the incubation, the complexes were washed five times with lysis buffer. The western blot was probed with mouse monoclonal NF1 antibody (Santa Cruz Biotechnology) and mouse monoclonal RAS antibody (Thermo Fisher Scientific).

Bioluminescence Resonance Energy Transfer (BRET) assay

Human embryonic kidney HEK293T cells were grown in DMEM/10% FBS without antibiotic treatment. Cells were seeded at 5 × 100 cells per well in a 96-well white opaque Perkin Elmer microplate. Twenty-four hours after seeding, cells were co-transfected with either a constant concentration of 0.1 μg of NF1-NanoLuc pcDNA expression plasmid or CRAF RBD-NanoLuc pcDNA expression plasmid with increasing concentrations of GFP-tagged KRAS (WT or Mutant) with 0.25 μl of Lipofectamine 2000 per well following the manufacturer's protocol (Thermo Fisher Scientific). Twenty-four hours later, medium was aspirated from each well and 25 μl of Nano-Glo Live Cell Reagent was added to each well per the manufacturer's protocol (Promega). Plates were placed on an orbital shaker for 1 min at 300 rpm. After incubation, the plate was read on the Tecan Infinite M200 PRO with LumiColor Dual Setting with an integration time of 1000 ms. BRET ratio was calculated from the dual emission readings. BRET ratio was plotted as a function of the RAS-GFP/NF1-NanoLuc plasmid ratio. BRET assays were repeated three times, each with eight biological replicates.

Excess Over Bliss Score

Cell proliferation index was converted to fraction affected (fA);(1 – percent viable)=fA. The predicted value (C) was calculated for each dose where A corresponds to fraction affected for cetuximab and B corresponds to fraction affected for AMG-510: C = (A+B) – (A x B). Excess over Bliss (EOB) was calculated as: EOB= ($fA_{(A+B)}$-C) x100, where $fA_{(A+B)}$ corresponds the fraction affected of combination of same dose of both Cetuximab and AMG-510.

Mathematical Model

Two models were used here. The first model does not include protein turnover (production and degradation) and is the version we developed previously (*18, 20*) and recently utilized to study KRAS G13D colorectal cancer and its response to cetuximab (*14*). We use this version of the model to study EGFR inhibition alone on KRAS G12C. The second model is an extension of the first that now includes protein production and protein degradation. We developed this model to study situations where protein turnover must also be considered, such as to study the effects of KRAS G12C inhibitors (*21*). The modeled half-life for RAS proteins (24 hours) is consistent with recent measurements (*13*). We use this version of the model to study combined treatment with KRAS G12C inhibitors and EGFR inhibitors. For both models, we model KRAS G12C to have impaired intrinsic GTPase activity (k_{GTPase} = 72% of the value of k_{GTPase} for WT RAS) (*22*), GAP mediated activation (k_{cat} equal to zero, with the assumption that codon 12, 13, and 61 RAS mutations are insensitive to GAPs (*50*), but with the GAP bound KRAS G12C-GTP protein still capable of intrinsic GTPase activity), and with a lower affinity for binding to RAS effectors (modeled as slightly faster dissociation from effectors, $k_{d,effector}$ = 120% of the value of $k_{d,effector}$ for WT RAS) (*22*), with all of these values based on previously published, experimental studies as cited. Based upon our detection of impaired binding to NF1 (Figure 3), we also modeled NF1 binding with an impaired binding to KRAS G12C ($K_{m,GAP}$ = 1000% of the value of $K_{m,GAP}$ for WT RAS). To study how alterations to effector binding, as suggested by previous studies (*22*) and by our studies (Figure 3), influence the response to EGFR inhibition we also evaluated further changes of 10× and 0.1× to the $k_{d,effector}$ parameter value. EGFR inhibitor dose responses are simulated with the assumption that EGFR mediated activation of RAS is driven by the recruitment of GEFs like SOS1 and SOS2 to activated EGFR, and that EGFR inhibition results in a reduction of this GEF mediated activation of RAS-GTP, as we have done previously (*14*). KRAS G12C inhibition is modeled as done previously (*21*). Model simulations are used to determine steady-state levels of total RAS-GTP (KRAS-GTP + NRAS-GTP + HRAS-GTP) as a measure of RAS pathway signal output. Simulations and analysis are performed in MATLAB (9.1.0.441655, MathWorks).

Figure 1. KRAS G12C colorectal cancer cells are partially sensitive to EGFR inhibition. (**A**) Colorectal SW48 isogenic cells harboring all KRAS WT or a heterozygous KRAS G12C, G12V, G12D mutant were treated with cetuximab at increasing doses and proliferation was measured by MTT cell viability assay 48 hours post treatment. IC50 doses are reported for sensitive cell lines. (**B**) Cell viability assay was confirmed by cell counting after treatment with cetuximab for 48 hours. (**C**) Colorectal cell lines SW837 (KRAS G12C/WT) and SW1463 (KRAS G12C/G12C) were treated with cetuximab at increasing doses and viability was measured by MTT assay 48 hours post treatment. (**D**) Cell viability was confirmed by cell counting assay 48 hours post treatment. MTT cell viability assays are representative of three experimental replicates, with eight biological replicates each. Data from one representative experiment are shown with error bars indicating standard deviation of the biological replicates. Cell counting assays were performed once to confirm MTT assays, and each treatment group was performed with twelve biological replicates. Individual data points, their means and standard deviations are presented for cell counting assays. Statistical significance tests were performed by using one-way ANOVA followed by post-hoc Tukey's for multiple comparisons. P Values are indicated.

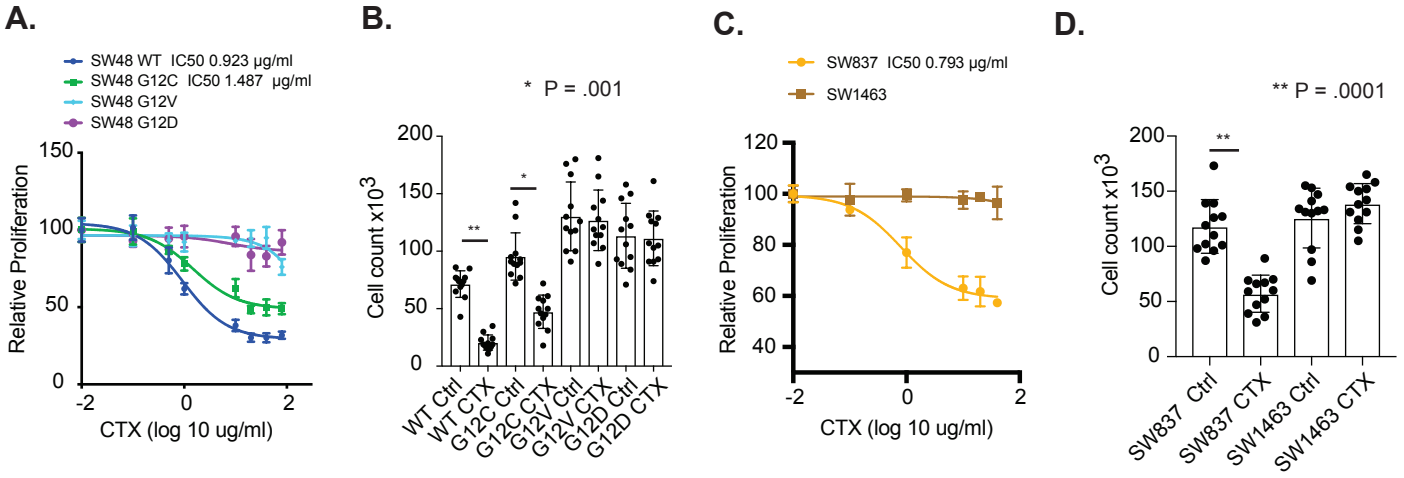
A.
SW48 WT IC50 0.923 µg/ml
SW48 G12C IC50 1.487 µg/ml
SW48 G12V
SW48 G12D
Relative Proliferation
CTX (log 10 ug/ml)
B.
* P = .001
Cell count x10^3
WT Ctrl
WT CTX
G12C Ctrl
G12C CTX
G12V Ctrl
G12V CTX
G12D Ctrl
G12D CTX
C.
SW837 IC50 0.793 µg/ml
SW1463
Relative Proliferation
CTX (log 10 ug/ml)
D.
** P = .0001
Cell count x10^3
SW837 Ctrl
SW837 CTX
SW1463 Ctrl
SW1463 CTX

Figure 1

Figure 2. Wild-type HRAS-GTP and NRAS-GTP are reduced upon EGFR inhibition. (**A**) SW48 isogenic cell lines were treated with cetuximab for 48 hours and then cell lysates were examined by active-RAS pulldown. IP product was probed for KRAS, HRAS, and NRAS with verified isoform specific antibodies by western blot. Input lysates were probed for pan-RAS, pERK, and ERK by western blot. Results are representative of three independent experiments. (**B**) Average infrared (IR) absorbance of KRAS, NRAS, and HRAS normalized to input signals from three independent experiments. (**C**) Average IR absorbance for pERK normalized to ERK from three independent experiments. (**D**) SW48 cells were treated with cetuximab for 48 hours prior to active-RAS pull down assay. IP products were purified and separated by isoelectric focusing and probed by western blot with a pan-RAS Antibody. (**E**) Average IR absorbance for each RAS isoform was calculated from three separate IEF experiments and normalized to KRAS. (**F**) Heterozygous KRAS G12C mutant SW837 and homozygous KRAS G12C mutant SW1463 cells were treated with cetuximab for 48 hours and then the active-RAS assay pull-down assay was performed. Results are representative of three independent experiments. (**G**) Average IR absorbances for each RAS isoform in the active-RAS pulldown assay from three independent experiments. (**H**) Average IR absorbance for each pERK normalized to total ERK signal from three independent experiments. (**I**) Heterozygous KRAS G12C mutant SW837 and homozygous KRAS G12C mutant SW1463 cells were treated with cetuximab for 48 hours prior to active-RAS pull down assay. The IP product was purified and separated by isoelectric focusing and probed with pan-RAS antibody. Results are representative of three independent experiments. (**J**) The average IR absorbance from three different IEF experiments with SW837 and SW1463 cells. Data sets with two treatment groups were analyzed with unpaired t-test. P-values are indicated within each panel and error bars represent standard deviation.

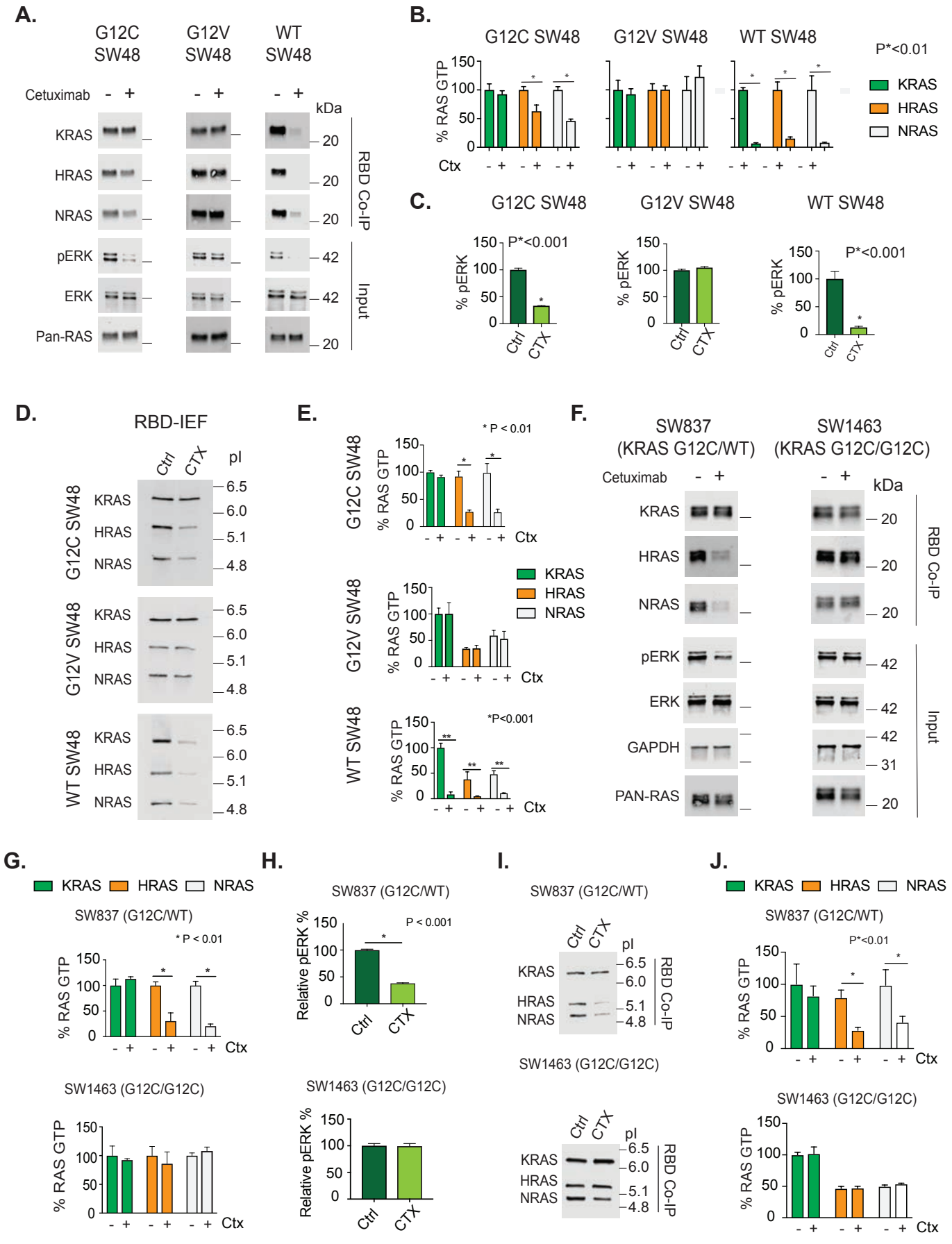
A.
G12C SW48
G12V SW48
WT SW48
Cetuximab - + - + - +
kDa
KRAS
HRAS
NRAS
pERK
ERK
Pan-RAS
20
20
20
42
42
20
RBD Co-IP
Input
B.
G12C SW48
G12V SW48
WT SW48
P*<0.01
% RAS GTP
150
100
50
0
Ctx
KRAS
HRAS
NRAS
C.
G12C SW48
G12V SW48
WT SW48
P*<0.001
% pERK
Ctrl
CTX
D.
RBD-IEF
Ctrl
CTX
pI
G12C SW48
G12V SW48
WT SW48
6.5
6.0
5.1
4.8
E.
* P < 0.01
*P<0.001
% RAS GTP
Ctx
KRAS
HRAS
NRAS
F.
SW837
(KRAS G12C/WT)
SW1463
(KRAS G12C/G12C)
Cetuximab - + - +
kDa
KRAS
HRAS
NRAS
pERK
ERK
GAPDH
PAN-RAS
20
20
20
42
42
42
31
20
RBD Co-IP
Input
G.
KRAS HRAS NRAS
SW837 (G12C/WT)
* P < 0.01
% RAS GTP
Ctx
SW1463 (G12C/G12C)
H.
SW837 (G12C/WT)
P < 0.001
Relative pERK %
Ctrl
CTX
SW1463 (G12C/G12C)
I.
SW837 (G12C/WT)
Ctrl
CTX
pI
KRAS
HRAS
NRAS
6.5
6.0
5.1
4.8
RBD Co-IP
SW1463 (G12C/G12C)
J.
KRAS HRAS NRAS
SW837 (G12C/WT)
P*<0.01
% RAS GTP
Ctx
SW1463 (G12C/G12C)

Figure 2

Figure 3. KRAS-G12C binds less well to NF1 and to CRAF. (**A**) HEK293T cells were transfected with increasing amount of KRAS-GFP expression plasmid and a constant concentration of NF1-NanoLuc. 24 hours post-transfection cells were treated with Nano-Glo Live Cell Reagent. BRET ratio was plotted as a function of RAS/NF1 expression plasmid ratio. BRET assays were performed with eight biological replicates, and were repeated three times. (**B**) Average BRET ratio from the three experiments at a RAS:NF1 ratio of 4:1. (**C**) HEK293T cells were transfected with either WT-KRAS-GFP, G12V-KRAS-GFP, G12C-KRAS GFP or NF1-FLAG expression plasmids. The NF1 co-IP mixing assay was performed and IP product and input lysate were probed by western blot for NF1, KRAS, and GFP. Results are representative of three independent experiments. (**D**) Average intensity of NF1 co-IP from the three independent experiments. (**E**) Isoelectric focused whole cell lysates from SW48 G12C, SW48 G12V and SW48 WT isogenic cells, probed with a pan-RAS antibody. Results are representative of three independent experiments. (**F**) Average proportions of KRAS, NRAS, and HRAS bound to RBD and in whole cell lysates from three separate IEF experiments. (**G**) Isoelectric focused whole cell lysates from heterozygous mutant KRAS G12C SW837 and homozygous mutant KRAS G12C SW1463 cells, probed with a pan-RAS antibody. Results are representative of three independent experiments. (**H**) Average proportions of KRAS, NRAS, and HRAS bound to and in whole cell lysates from three separate IEF experiments. (**I**) HEK293T cells were transfected with increasing concentrations of KRAS-GFP expression plasmids and a constant concentration of CRAF-RBD-NanoLuc. 24 hours post-transfection cells were treated with Nano-Glo Live Cell Reagent. BRET ratio was plotted as a function of RAS/NF1 expression plasmid ratio. BRET assays were performed with three experimental replicates, each containing eight biological replicates. (**J**) Average BRET ratio from the three experiments at a RAS:RBD ratio of 2:1. (**K**) SW48 Isogenic cells were harvested and prepared for RAF-RBD pulldown assay, one set was not exposed to γ-S-GTP and the other was incubated in γ-S-GTP for 20 minutes. IP-product and input were probed by western blot for KRAS and GAPDH. Results are representative of three independent experiments. (**L**) Average quantity of KRAS WT, KRAS G12C, and KRAS G12C pulled down by RAF-RBD from three independent experiments. All experiments were performed three times. Treatment groups were analyzed by one-way ANOVA followed by post-hoc Tukey's test for multiple comparisons and P-values are indicated. Error bars in all panels represent standard deviation.

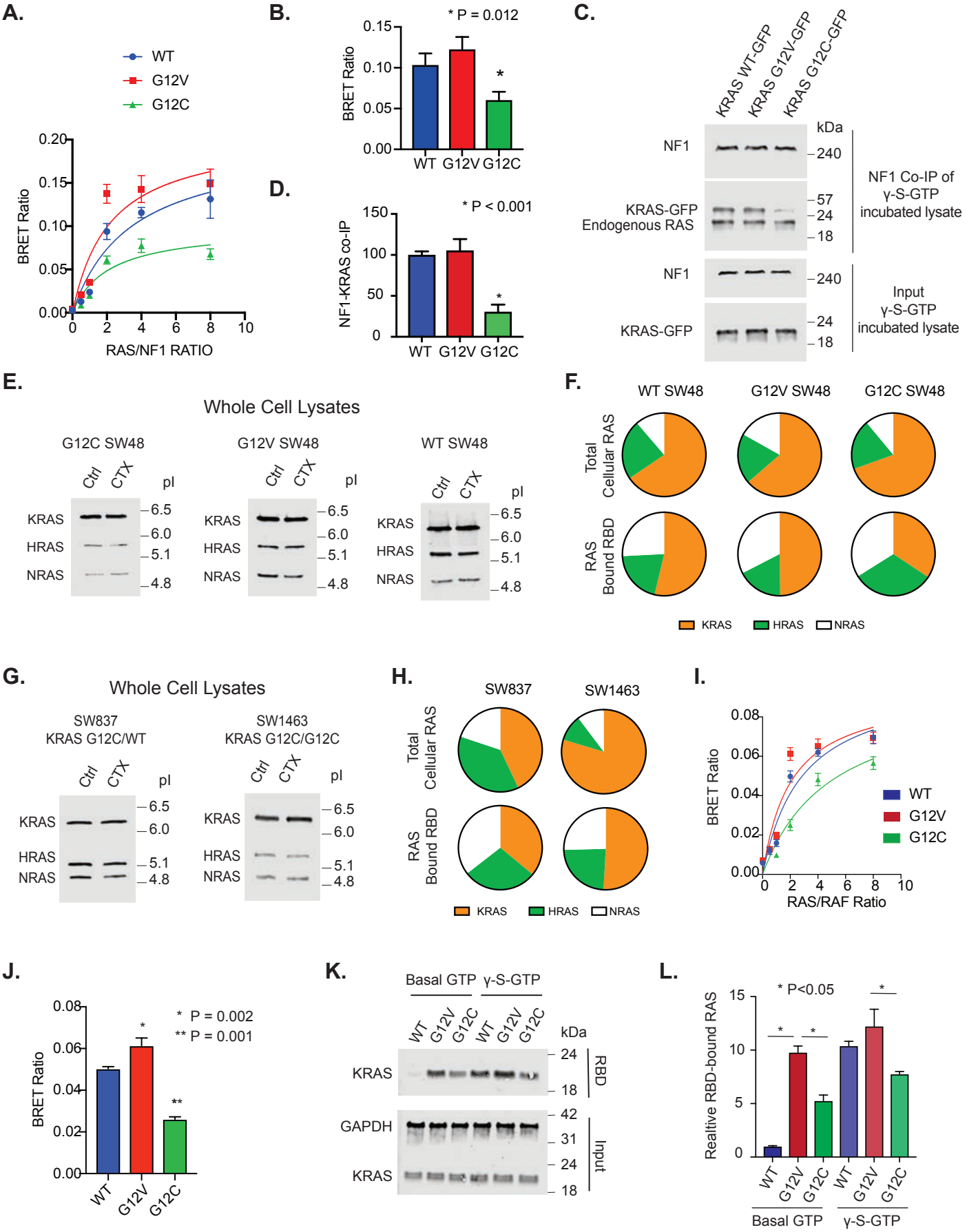
A.
WT
G12V
G12C
BRET Ratio
RAS/NF1 RATIO
B.
* P = 0.012
BRET Ratio
WT G12V G12C
C.
KRAS WT-GFP
KRAS G12V-GFP
KRAS G12C-GFP
kDa
NF1
KRAS-GFP
Endogenous RAS
NF1 Co-IP of γ-S-GTP incubated lysate
Input γ-S-GTP incubated lysate
D.
* P < 0.001
NF1-KRAS co-IP
WT G12V G12C
E.
Whole Cell Lysates
G12C SW48
G12V SW48
WT SW48
Ctrl
CTX
pI
KRAS
HRAS
NRAS
F.
WT SW48
G12V SW48
G12C SW48
Total Cellular RAS
RAS Bound RBD
KRAS
HRAS
NRAS
G.
Whole Cell Lysates
SW837
KRAS G12C/WT
SW1463
KRAS G12C/G12C
H.
SW837
SW1463
I.
BRET Ratio
RAS/RAF Ratio
WT
G12V
G12C
J.
* P = 0.002
** P = 0.001
K.
Basal GTP
γ-S-GTP
RBD
Input
GAPDH
L.
* P<0.05
Realtive RBD-bound RAS
Basal GTP
γ-S-GTP

Figure 3

Figure 4. Mathematical modeling supports KRAS G12C cells being sensitive to cetuximab. (**A**) Simulated anti-EGFR dose responses from the computational RAS model for KRAS G12C modeled with a reduced affinity for NF1 (blue) or without a reduced affinity for NF1 (black). For comparison, G12D (green dotted line), G13D (red dotted line), and WT (black dotted line) are also presented in this and the other panels. (**B**) Simulated anti-EGFR dose responses from the RAS model, further subdivided to reveal the change in mutant RAS-GTP (left) and in WT RAS (right). (**C**) Simulated anti-EGFR dose responses for modeled heterozygous (blue) and modeled heterozygous (light blue) conditions, both with a reduced affinity for NF1. (**D**) Simulated anti-EGFR dose responses for heterozygous G12C mutant conditions with an order of magnitude decrease and increase (grey), respectively above and below G12C (blue).

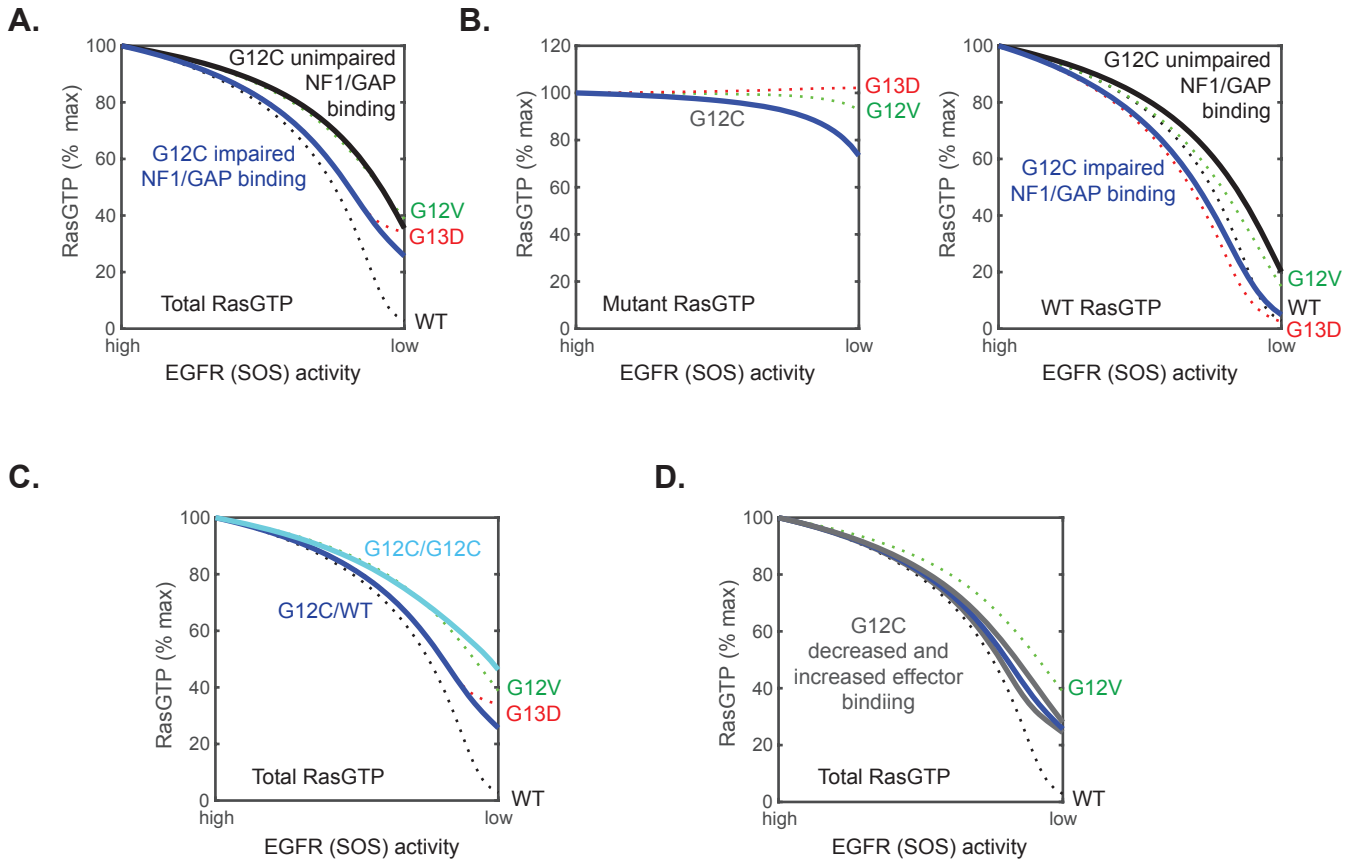
A.
B.
C.
D.
RasGTP (% max)
EGFR (SOS) activity
high
low
G12C unimpaired NF1/GAP binding
G12C impaired NF1/GAP binding
Total RasGTP
G12V
G13D
WT
G12C
Mutant RasGTP
WT RasGTP
G12C/G12C
G12C/WT
G12C decreased and increased effector bindiing

Figure 4

Figure 5. AMG-510 prevents KRAS-G12C from interacting with NF1 and CRAF. (**A**) SW48 isogenic cell lines, SW837 and SW1463 were treated with increasing doses of AMG-510 for 48 hours and cell viability was measured with the MTT assay. Data points represent the mean of eight biological replicates. Results are representative of three separate experiments. (**B**) HEK293T cells were co-transfected with KRAS-GFP and NF1-NanoLuc with and without 500nM AMG-510 for 24 hours and signal is represented as a BRET ratio for both sample groups. Bars represent the mean of eight biological replicates. Results are representative of an individual experiment from three separate experiments. (**C**) HEK293T cells were co-transfected with KRAS-GFP and CRAF-NanoLuc with and without 500nM AMG-510 for 24 hours and signal is represented as a BRET ratio for both sample groups. Bars represent the mean of eight biological replicates. Results are representative of an individual experiment from three separate experiments. (**D**). HEK293T cells were transfected with either KRAS-G12C-GFP and NF1, NF1 alone, or mock transfection. Cells were then treated with either vehicle or 500 nM AMG-510 for 24 hours. Results are representative of an individual experiment from three separate experiments. (**E**) Mean KRAS G12C pull-down for the three independent NF1-coIP experiments. Statistical analysis was performed with unpaired t-test and P-values are indicated. Error bars in all panels represent standard deviation.

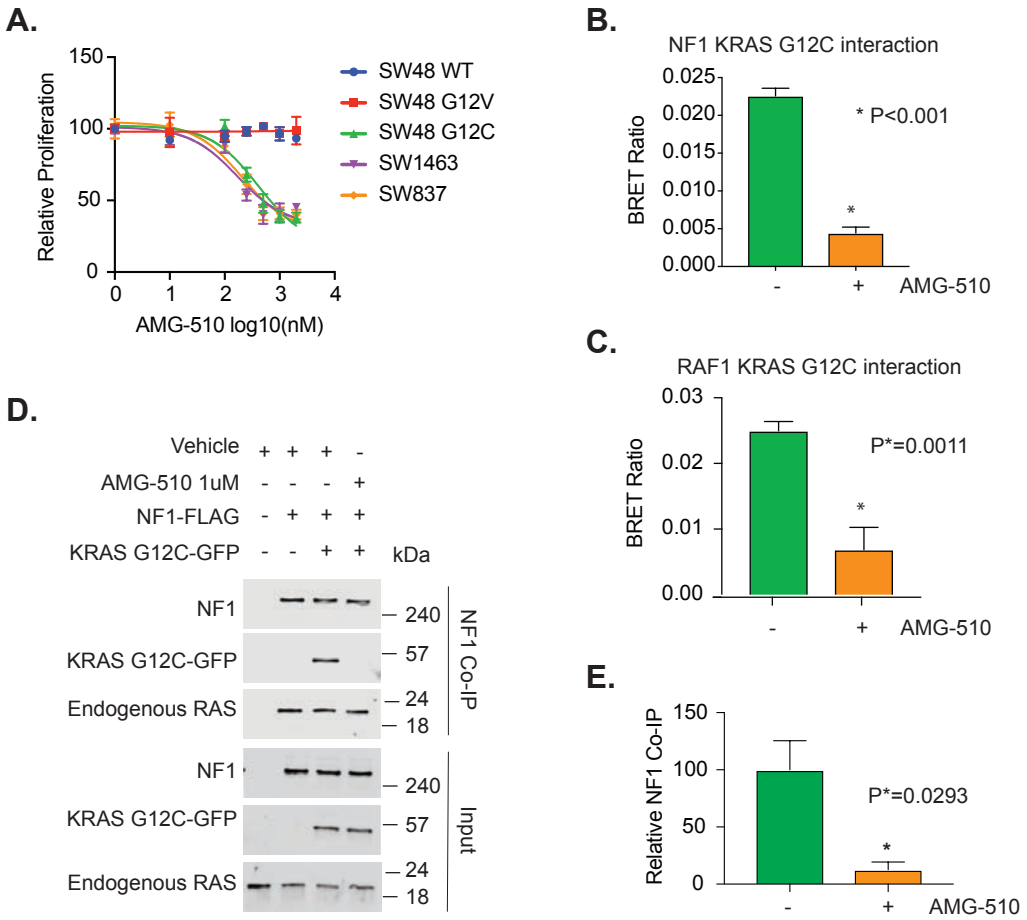
A.
Relative Proliferation
150
100
50
0
0
1
2
3
4
AMG-510 log10(nM)
SW48 WT
SW48 G12V
SW48 G12C
SW1463
SW837
B.
NF1 KRAS G12C interaction
BRET Ratio
0.025
0.020
0.015
0.010
0.005
0.000
* P<0.001
*
-
+
AMG-510
C.
RAF1 KRAS G12C interaction
BRET Ratio
0.03
0.02
0.01
0.00
P*=0.0011
*
-
+
AMG-510
D.
Vehicle + + + -
AMG-510 1uM - - - +
NF1-FLAG - + + +
KRAS G12C-GFP - - + +
kDa
NF1
KRAS G12C-GFP
Endogenous RAS
240
57
24
18
NF1 Co-IP
NF1
KRAS G12C-GFP
Endogenous RAS
240
57
24
18
Input
E.
Relative NF1 Co-IP
150
100
50
0
P*=0.0293
*
-
+
AMG-510

Figure 5

Figure 6. AMG-510 and cetuximab synergize to decrease cell viability at lower effective doses when compared to single-agent therapy. (**A**) Cellular proliferation as measured by the MTT assay for SW48 isogenic cells, SW1463, and SW837 treated with combinations of cetuximab and AMG-510 for 48 hours. Heatmaps present average values from three separate experiments. (**B**) Calculated Excess over Bliss (EOB) synergy scores for the data in (A).

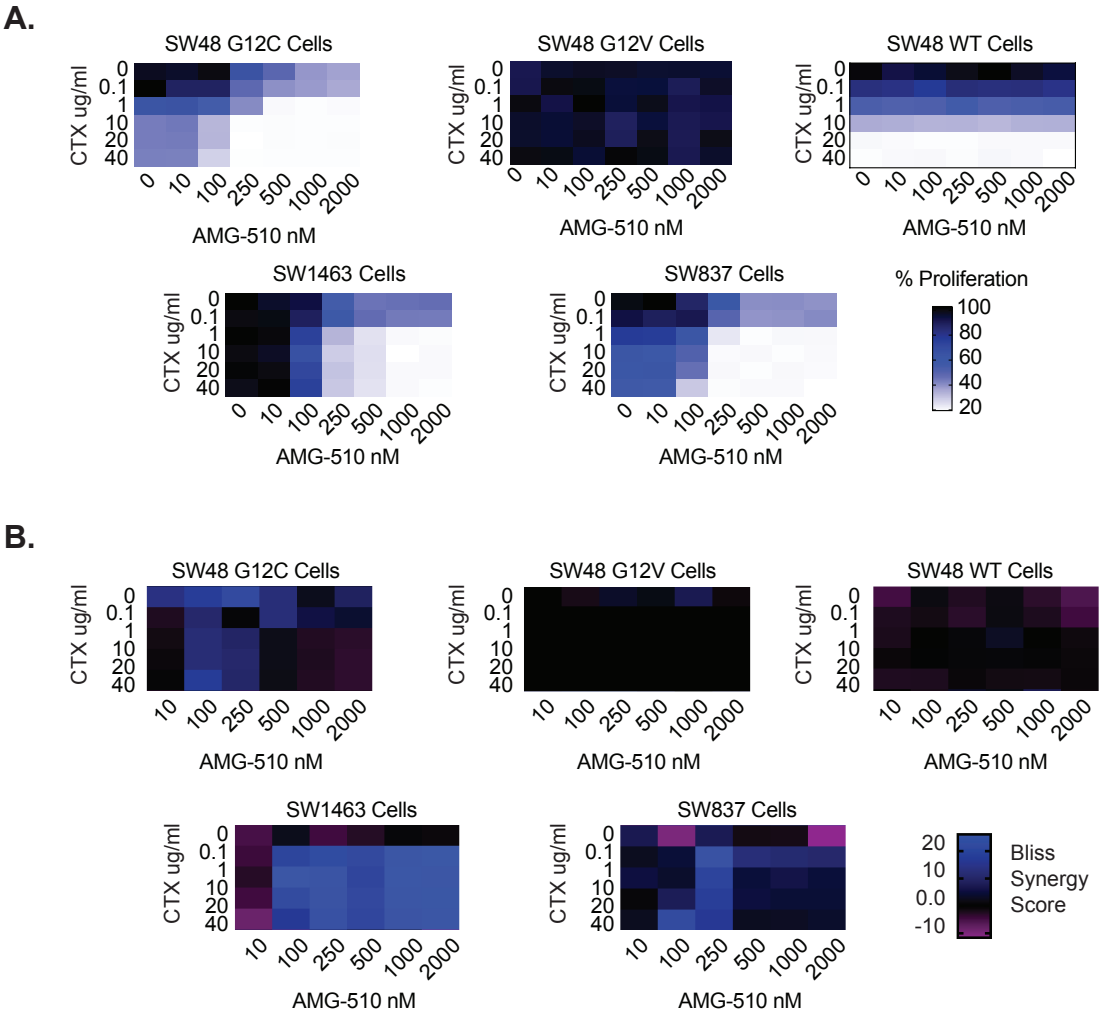
A.
SW48 G12C Cells
SW48 G12V Cells
SW48 WT Cells
SW1463 Cells
SW837 Cells
CTX ug/ml
0
0.1
1
10
20
40
AMG-510 nM
0
10
100
250
500
1000
2000
% Proliferation
100
80
60
40
20
B.
Bliss
Synergy
Score
20
10
0.0
-10

Figure 6

Figure 7. Mathematical modeling suggests synergy between G12C and EGFR inhibitors that follows from co-targeting wild-type and mutant RAS. (**A**) Model-predicted Excess over Bliss (EOB) synergy scores based on predicted total RAS-GTP for the combination of KRAS G12C inhibition and EGFR inhibition. Total RAS-GTP level predictions were obtained from simulations of the KRAS G12C parameterized RAS model that includes protein production and turnover. (**B**) Model-predicted EOB synergy scores based on predicted mutant RAS-GTP levels. (**C**) Model-predicted EOB scores based on predicted WT RAS-GTP levels.

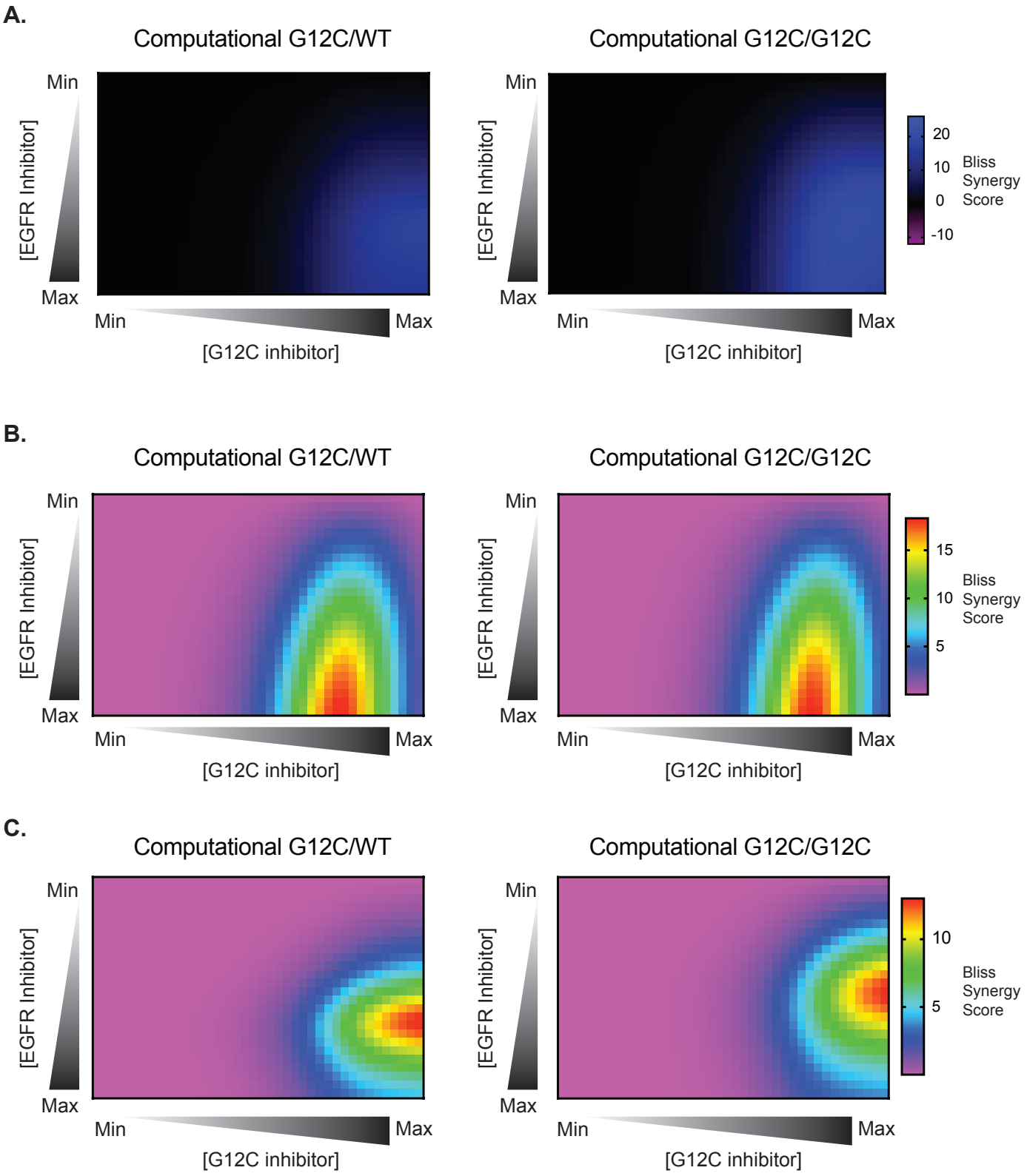
A.
Computational G12C/WT
Computational G12C/G12C
Min
Max
[EGFR Inhibitor]
[G12C inhibitor]
20
10
0
-10
Bliss Synergy Score
B.
Computational G12C/WT
Computational G12C/G12C
15
10
5
Bliss Synergy Score
C.
Computational G12C/WT
Computational G12C/G12C
10
5
Bliss Synergy Score

Figure 7

Figure 8. The combination of AMG-510 and cetuximab results in profound suppression of wild-type RAS-GTP. (**A**) Active RAS measurements by RBD-WB for SW837 and SW1463 cells treated either with vehicle, 1μg/ml cetuximab, 250nM AMG-510 or both 1μg/ml cetuximab and 250nM AMG-510 for 48 hours. Results are representative of three separate experiments. (**B**) Mean RAS-GTP levels from three RBD-WB RBD pulldown assays with standard deviation. (**C**) Mean pERK signal from the input lysates for the three RBD-WB experiments with standard deviation. (**D**) SW48-G12C cells were treated with 250nM of AMG-510 with and without cetuximab pretreatment for 24 hours (1μg/ml). Cells were isolated at 0, 6, 12, 24, and 48 hours after AMG-10 treatment and KRAS-, NRAS-, and HRAS-GTP levels were assessed by RBD-IEF. Results are representative of two separate experiments.

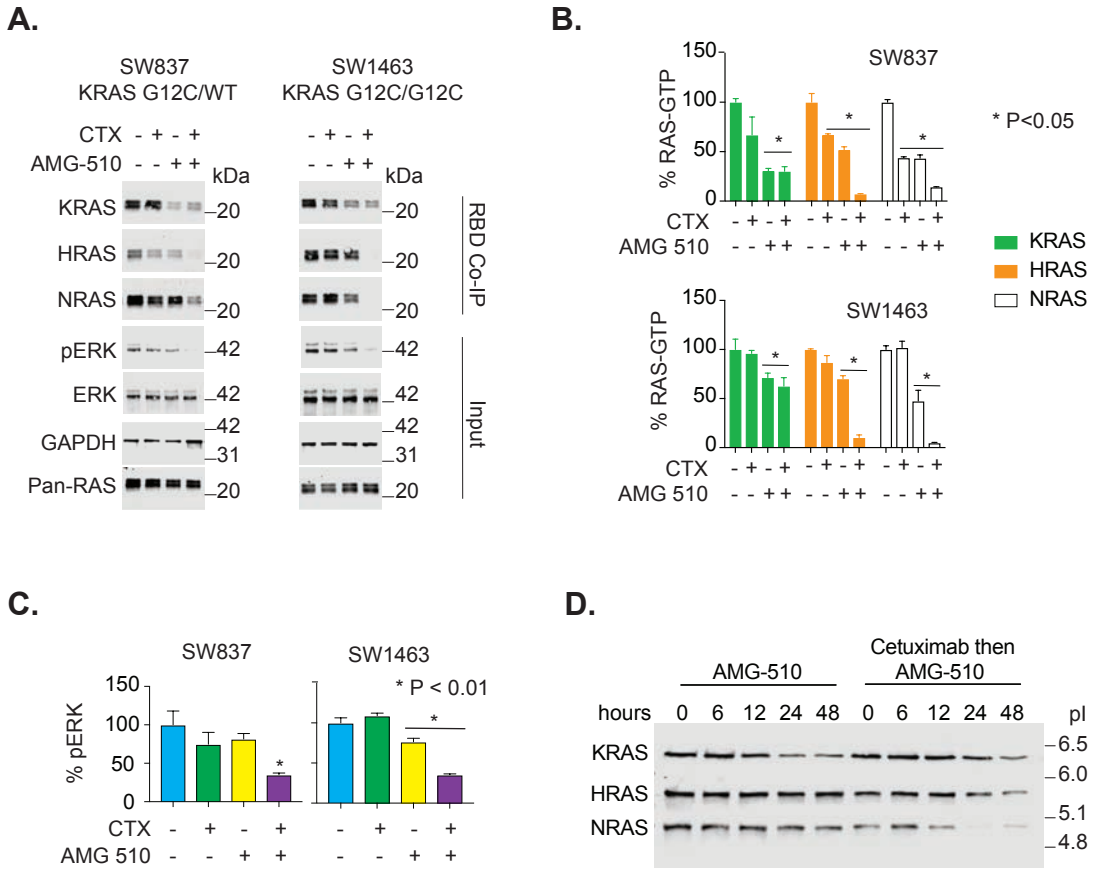
A.
SW837
KRAS G12C/WT
SW1463
KRAS G12C/G12C
CTX
AMG-510
kDa
KRAS
HRAS
NRAS
pERK
ERK
GAPDH
Pan-RAS
RBD Co-IP
Input
B.
SW837
SW1463
% RAS-GTP
* P<0.05
KRAS
HRAS
NRAS
C.
SW837
SW1463
% pERK
* P < 0.01
D.
AMG-510
Cetuximab then AMG-510
hours
pI

Figure 8

REFERENCES

1. D. J. Jonker *et al.*, Cetuximab for the treatment of colorectal cancer. *N Engl J Med* **357**, 2040-2048 (2007).
2. E. Van Cutsem *et al.*, Open-label phase III trial of panitumumab plus best supportive care compared with best supportive care alone in patients with chemotherapy-refractory metastatic colorectal cancer. *J Clin Oncol* **25**, 1658-1664 (2007).
3. J. M. Ostrem, K. M. Shokat, Direct small-molecule inhibitors of KRAS: from structural insights to mechanism-based design. *Nat Rev Drug Discov* **15**, 771-785 (2016).
4. N. Cancer Genome Atlas, Comprehensive molecular characterization of human colon and rectal cancer. *Nature* **487**, 330-337 (2012).
5. A. D. Cox, S. W. Fesik, A. C. Kimmelman, J. Luo, C. J. Der, Drugging the undruggable RAS: Mission possible? *Nat Rev Drug Discov* **13**, 828-851 (2014).
6. N. Cancer Genome Atlas Research, Comprehensive molecular profiling of lung adenocarcinoma. *Nature* **511**, 543-550 (2014).
7. E. Cerami *et al.*, The cBio cancer genomics portal: an open platform for exploring multidimensional cancer genomics data. *Cancer Discov* **2**, 401-404 (2012).
8. J. Gao *et al.*, Integrative analysis of complex cancer genomics and clinical profiles using the cBioPortal. *Sci Signal* **6**, pl1 (2013).
9. C. S. Karapetis *et al.*, K-ras mutations and benefit from cetuximab in advanced colorectal cancer. *N Engl J Med* **359**, 1757-1765 (2008).
10. J. M. Ostrem, U. Peters, M. L. Sos, J. A. Wells, K. M. Shokat, K-Ras(G12C) inhibitors allosterically control GTP affinity and effector interactions. *Nature* **503**, 548-551 (2013).
11. J. C. Hunter *et al.*, In situ selectivity profiling and crystal structure of SML-8-73-1, an active site inhibitor of oncogenic K-Ras G12C. *Proc Natl Acad Sci U S A* **111**, 8895-8900 (2014).
12. J. Canon *et al.*, The clinical KRAS(G12C) inhibitor AMG 510 drives anti-tumour immunity. *Nature*, (2019).
13. J. G. Christensen *et al.*, The KRASG12C Inhibitor, MRTX849, Provides Insight Toward Therapeutic Susceptibility of KRAS Mutant Cancers in Mouse Models and Patients. *Cancer Discov*, (2019).
14. T. McFall *et al.*, A systems mechanism for KRAS mutant allele-specific responses to targeted therapy. *Sci Signal* **12**, (2019).
15. W. De Roock *et al.*, Association of KRAS p.G13D mutation with outcome in patients with chemotherapy-refractory metastatic colorectal cancer treated with cetuximab. *JAMA* **304**, 1812-1820 (2010).
16. C. J. Mageean, J. R. Griffiths, D. L. Smith, M. J. Clague, I. A. Prior, Absolute Quantification of Endogenous Ras Isoform Abundance. *PLoS One* **10**, e0142674 (2015).
17. E. C. Stites, Differences in sensitivity to EGFR inhibitors could be explained by described biochemical differences between oncogenic Ras mutants. *bioRxiv* **https://doi.org/10.1101/005397**, (2014).
18. E. C. Stites, P. C. Trampont, Z. Ma, K. S. Ravichandran, Network analysis of oncogenic Ras activation in cancer. *Science* **318**, 463-467 (2007).
19. E. C. Stites, K. S. Ravichandran, Mathematical investigation of how oncogenic ras mutants promote ras signaling. *Methods Mol Biol* **880**, 69-85 (2012).
20. E. C. Stites, P. C. Trampont, L. B. Haney, S. F. Walk, K. S. Ravichandran, Cooperation between Noncanonical Ras Network Mutations. *Cell Rep* **10**, 307-316 (2015).

21. E. C. Stites, A. S. Shaw, Quantitative Systems Pharmacology Analysis of KRAS G12C Covalent Inhibitors. *CPT Pharmacometrics Syst Pharmacol* **7**, 342-351 (2018).
22. J. C. Hunter *et al.*, Biochemical and Structural Analysis of Common Cancer-Associated KRAS Mutations. *Mol Cancer Res* **13**, 1325-1335 (2015).
23. M. P. Patricelli *et al.*, Selective Inhibition of Oncogenic KRAS Output with Small Molecules Targeting the Inactive State. *Cancer Discov* **6**, 316-329 (2016).
24. P. Lito, M. Solomon, L. S. Li, R. Hansen, N. Rosen, Allele-specific inhibitors inactivate mutant KRAS G12C by a trapping mechanism. *Science* **351**, 604-608 (2016).
25. S. Misale *et al.*, KRAS G12C NSCLC Models Are Sensitive to Direct Targeting of KRAS in Combination with PI3K Inhibition. *Clin Cancer Res* **25**, 796-807 (2019).
26. K. Lou *et al.*, KRAS(G12C) inhibition produces a driver-limited state revealing collateral dependencies. *Sci Signal* **12**, (2019).
27. I. Yen *et al.*, Pharmacological Induction of RAS-GTP Confers RAF Inhibitor Sensitivity in KRAS Mutant Tumors. *Cancer Cell* **34**, 611-625 e617 (2018).
28. G. A. Hobbs, A. Wittinghofer, C. J. Der, Selective Targeting of the KRAS G12C Mutant: Kicking KRAS When It's Down. *Cancer Cell* **29**, 251-253 (2016).
29. K. D. Westover, P. A. Janne, N. S. Gray, Progress on Covalent Inhibition of KRAS(G12C). *Cancer Discov* **6**, 233-234 (2016).
30. H. P. Moll *et al.*, Afatinib restrains K-RAS-driven lung tumorigenesis. *Sci Transl Med* **10**, (2018).
31. J. W. Keller *et al.*, Oncogenic K-RAS subverts the antiapoptotic role of N-RAS and alters modulation of the N-RAS:gelsolin complex. *Oncogene* **26**, 3051-3059 (2007).
32. K. H. Lim, B. B. Ancrile, D. F. Kashatus, C. M. Counter, Tumour maintenance is mediated by eNOS. *Nature* **452**, 646-649 (2008).
33. H. H. Jeng, L. J. Taylor, D. Bar-Sagi, Sos-mediated cross-activation of wild-type Ras by oncogenic Ras is essential for tumorigenesis. *Nat Commun* **3**, 1168 (2012).
34. A. Young, D. Lou, F. McCormick, Oncogenic and wild-type Ras play divergent roles in the regulation of mitogen-activated protein kinase signaling. *Cancer Discov* **3**, 112-123 (2013).
35. C. Bentley *et al.*, A requirement for wild-type Ras isoforms in mutant KRas-driven signalling and transformation. *Biochem J* **452**, 313-320 (2013).
36. E. Grabocka *et al.*, Wild-type H- and N-Ras promote mutant K-Ras-driven tumorigenesis by modulating the DNA damage response. *Cancer Cell* **25**, 243-256 (2014).
37. B. Zhou, C. J. Der, A. D. Cox, The role of wild type RAS isoforms in cancer. *Semin Cell Dev Biol* **58**, 60-69 (2016).
38. M. P. Muller, S. Jeganathan, A. Heidrich, J. Campos, R. S. Goody, Nucleotide based covalent inhibitors of KRas can only be efficient in vivo if they bind reversibly with GTP-like affinity. *Sci Rep* **7**, 3687 (2017).
39. R. S. Goody, M. P. Muller, D. Rauh, Mutant-Specific Targeting of Ras G12C Activity by Covalently Reacting Small Molecules. *Cell Chem Biol* **26**, 1338-1348 (2019).
40. M. P. Morelli, S. Kopetz, Hurdles and complexities of codon 13 KRAS mutations. *J Clin Oncol* **30**, 3565-3567 (2012).
41. S. Kopetz *et al.*, Phase II Pilot Study of Vemurafenib in Patients With Metastatic BRAF-Mutated Colorectal Cancer. *J Clin Oncol* **33**, 4032-4038 (2015).

42. R. B. Corcoran *et al.*, EGFR-mediated re-activation of MAPK signaling contributes to insensitivity of BRAF mutant colorectal cancers to RAF inhibition with vemurafenib. *Cancer Discov* **2**, 227-235 (2012).
43. A. Prahallad *et al.*, Unresponsiveness of colon cancer to BRAF(V600E) inhibition through feedback activation of EGFR. *Nature* **483**, 100-103 (2012).
44. S. J. Heidorn *et al.*, Kinase-dead BRAF and oncogenic RAS cooperate to drive tumor progression through CRAF. *Cell* **140**, 209-221 (2010).
45. P. I. Poulikakos, C. Zhang, G. Bollag, K. M. Shokat, N. Rosen, RAF inhibitors transactivate RAF dimers and ERK signalling in cells with wild-type BRAF. *Nature* **464**, 427-430 (2010).
46. G. Hatzivassiliou *et al.*, RAF inhibitors prime wild-type RAF to activate the MAPK pathway and enhance growth. *Nature* **464**, 431-435 (2010).
47. R. B. Corcoran *et al.*, Combined BRAF, EGFR, and MEK Inhibition in Patients with BRAF(V600E)-Mutant Colorectal Cancer. *Cancer Discov* **8**, 428-443 (2018).
48. S. Kopetz *et al.*, Encorafenib, Binimetinib, and Cetuximab in BRAF V600E-Mutated Colorectal Cancer. *N Engl J Med* **381**, 1632-1643 (2019).
49. E. C. Stites, The response of cancers to BRAF inhibition underscores the importance of cancer systems biology. *Sci Signal* **5**, pe46 (2012).
50. A. G. Stephen, D. Esposito, R. K. Bagni, F. McCormick, Dragging ras back in the ring. *Cancer Cell* **25**, 272-281 (2014).